

High-Order Mode of Spoof Surface Plasmon Polaritons and Its Application in Bandpass Filters

Kai-Da Xu¹, Senior Member, IEEE, Sen Lu, Ying-Jiang Guo, and Qiang Chen², Senior Member, IEEE

Abstract—A bandpass filter (BPF) with a notched band is designed based on the high-order mode of spoof surface plasmon polaritons (SSPPs). The high-efficiency passband is developed from the first high-order mode (Mode 1) of SSPPs. Compared with the fundamental mode having low-pass response, the Mode 1 has the inherent bandpass response; thus, the BPF generated by Mode 1 does not need to add an additional high-pass filtering structure and employ a gradient transition structure for excitation. The Mode 1 of SSPPs can be effectively excited just with a simple trapezoidal transition converting the signals from microstrip line to SSPP waveguide. Moreover, by embedding a U-shaped resonator into the SSPP structure, a BPF with a notched band is constructed, where the location of the notched band will be red-shifted as the length of resonator increases. The measurements of two fabricated prototypes agree with the simulated ones, which verify the feasibility of our design.

Index Terms—Bandpass filter (BPF), high-order mode, notched band, spoof surface plasmon polaritons (SSPPs).

I. INTRODUCTION

SURFACE plasmon polaritons (SPPs) have been recently one of the most popular topics in modern physics and technology [1]–[4], which can be effectively excited and propagated while decayed exponentially into the interface. With the ability of strong confinement, the SPPs can break the diffraction limit and localize the wave in subwavelength scale [5], [6]. At low frequencies, metals resemble perfect electric conductors (PECs) that cannot support the natural SPPs. Therefore, a kind of plasmonic metamaterials with periodic subwavelength structures is developed, which can support the SPP-like surface wave at microwave [7]–[9] and

terahertz [10]–[12] regimes, namely, spoof SPPs (SSPPs). The dispersion characteristics of SSPPs can be tailored by the geometrical parameters of the periodic structures. After the experimental validation that the SSPP modes can be effectively supported by the planar structures [13], [14] and well matched with the guided waves [15], numerous planar SSPPs have been proposed for different applications, such as sensors [16], filters [17], [18], antennas [19], power dividers [20], and frequency splitters [21].

The abovementioned components are investigated and designed based on the fundamental mode of SSPPs, which usually need extra gradient transitions with large space occupation. As for the high-order mode of SSPPs, double grating SSPP structures [22], [23] and single grating ones [24], [25] were investigated. For instance, two different broadband symmetric SSPP waveguides with reduced transversal sizes were designed using high-order modes based on T-shaped complementary grooves [22] and split-ring grooves [23], respectively.

Also, in some practical cases, the undesired signals from external sources may exist within the passband which will deteriorate the performance of the system. To suppress the unwanted signals, several filters with notched bands are implemented [26]–[29], which are all constructed by introducing the resonators inside the SSPP waveguides to reject the specific frequencies. Especially in [27], with the mounting active components, the notch can be electronically tuned by adjusting the applied bias voltage across the varactor diode.

In this article, a high-efficiency passband developed from the first high-order mode (Mode 1) of simple SSPP waveguide is excited, and a bandpass filter (BPF) with a notched band is further designed. First, the properties of the fundamental mode (Mode 0) and Mode 1 of the single grating metallic strip SSPP structure are studied. Compared with the Mode 0 having the low-pass response, the Mode 1 has the inherent bandpass response. Meanwhile, with very simple trapezoidal transition, the Mode 1 of SSPPs will be effectively excited, and thus the passband is generated with good transmission performance. Second, through embedding a U-shaped resonator into the SSPP structure, a notched band occurs within the passband.

II. HIGH-ORDER MODE OF SSPPS AND BPF APPLICATION

A. High-Order Mode of SSPPs

In this subsection, we first investigate the fundamental mode (Mode 0) and the first high-order mode (Mode 1) of the single grating metallic strip SSPP structure. Then, with

Manuscript received September 2, 2020; revised November 9, 2020; accepted December 7, 2020. Date of publication December 22, 2020; date of current version January 11, 2021. This work was supported in part by the FY2019 JSPS Postdoctoral Fellowship for Research in Japan under Grant P19350 and in part by the Grant-in-Aid for JSPS Research Fellow under Grant JP19F19350. The review of this article was arranged by Senior Editor D. A. Shiffler. (Corresponding author: Kai-Da Xu.)

Kai-Da Xu is with the School of Information and Communications Engineering, Xi'an Jiaotong University, Xi'an 710049, China, and also with the Department of Communications Engineering, Tohoku University, Sendai 980-8579, Japan (e-mail: kaidaxu@ieee.org).

Sen Lu is with the Department of Electronic Science, Xiamen University, Xiamen 361005, China.

Ying-Jiang Guo is with the Microsystem and Terahertz Research Center, China Academy of Engineering Physics, Chengdu 610200, China.

Qiang Chen is with the Department of Communications Engineering, Tohoku University, Sendai 980-8579, Japan.

Color versions of one or more figures in this article are available at <https://doi.org/10.1109/TPS.2020.3043889>.

Digital Object Identifier 10.1109/TPS.2020.3043889

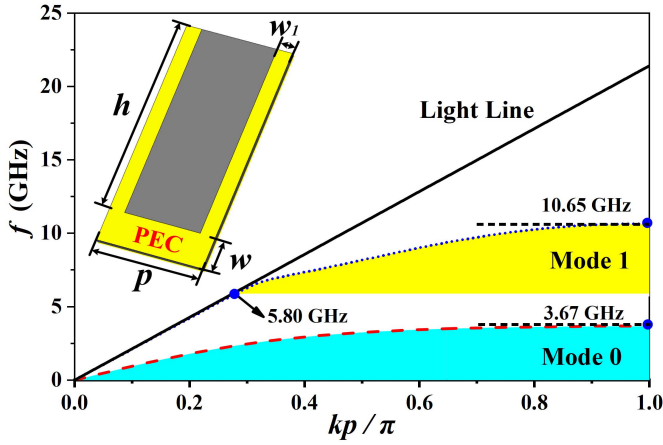


Fig. 1. Simulated dispersion curves for the first two modes of the single grating metallic strip SSPP structure. The inset is the schematic of the SSPP unit cell with the geometric parameters of $p = 7$ mm, $w = 2.2$ mm, $h = 13$ mm, and $w_1 = 1$ mm. k is the wavenumber. The front and back metal parts are set as PECs attached on two sides of the Rogers 5880 substrate ($\epsilon_r = 2.2$, $\tan \delta = 0.0009$) with thickness of 0.508 mm.

simple trapezoidal transition, the Mode 1 of the SSPPs can be effectively excited, and thus a passband is generated with good transmission performance.

The proposed single grating metallic strip SSPP structure is designed on the Rogers RT/Duroid 5880 substrate [30], as shown in the inset of Fig. 1. The back of the substrate is designed as the metallic ground plane to further enhance the electromagnetic field confinement. Due to the metal usually seen as the PEC at microwave frequency, we assume the metal in this SSPP structure as the PEC with zero thickness in simulation. As derived in [24] and [25], the single grating SSPP structure can support high-order modes of SSPPs when the depth of groove h is larger than the period p , and the number (N) of SSPP modes can be expressed by

$$N = 1 + \text{int}(h/p) \quad (1)$$

where $\text{int}(h/p)$ represents the integer part of the h/p .

Following the eigenmode simulation settings introduced in [31], Fig. 1 shows the simulated dispersion relations of this SSPP structure using software CST Microwave Studio as well as the light line in free space for reference. The k in Fig. 1 denotes the propagation constant. In this configuration, two SSPP modes exist, i.e., Mode 0 and Mode 1. According to the dispersion curves, both of the two SSPP modes start from the point of intersection with light line and then gradually deviate from the light line until approaching the maximal frequency value, i.e., the asymptotic frequency. The field confinement becomes better as it approaches to the asymptotic frequency. It should be noted that the Mode 0 and Mode 1 have no overlapping part, indicating the single mode propagation is available for each mode, which is different from the traditional rectangular waveguide.

To understand the two SSPP modes clearly, the normalized electric field distributions at their asymptotic frequencies 3.67 and 10.65 GHz are plotted in Fig. 2, following the method in [23]. It can be observed that the electromagnetic energy is

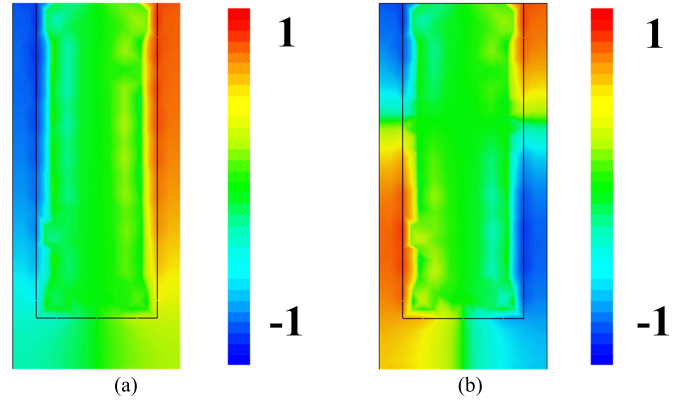


Fig. 2. Normalized electric field distributions of (a) Mode 0 and (b) Mode 1 at their asymptotic frequencies 3.67 and 10.65 GHz, respectively. The color bar indicates the electric field polarity and field strength in logarithm.

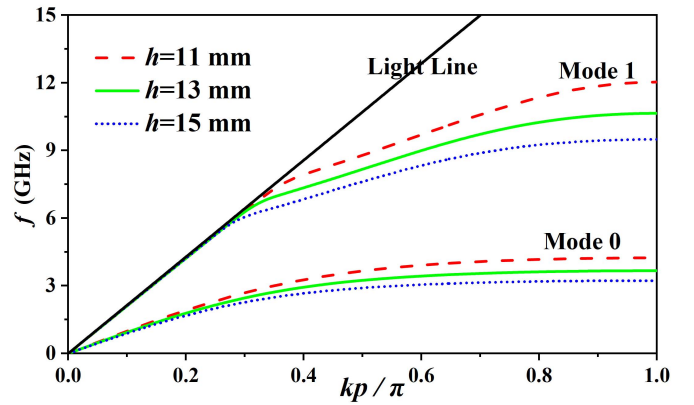


Fig. 3. Simulated dispersion curves of the SSPP structure with different groove depths h , where $p = 7$ mm, $w = 2.2$ mm, and $w_1 = 1$ mm.

concentrated along the two sides of the metallic strips, and the field strength is symmetric but with the opposite polarity. The difference between the two SSPP modes is that the Mode 0 has one electric polarity, while the Mode 1 has two electric polarities at one metallic strip.

In the previous reported works, the fundamental mode (Mode 0) has been well studied and the groove depth h is of significance effect on it. Compared with the Mode 0 having low-pass response, the Mode 1 has the inherent bandpass response; thus, the BPF generated by Mode 1 does not need to add an additional high-pass filtering structure and employ a gradient transition structure for excitation. In this article, we further study the property of the Mode 1 and the impact of h on it. As shown in Fig. 3, generally, the Mode 1 can realize a bandpass filtering function without the interference from Mode 0. As the parameter h increases from 11 to 15 mm with step of 2 mm, the point of intersection with the light line (i.e., lower cutoff frequency) and the asymptotic frequency (i.e., upper cutoff frequency) are decreased simultaneously. Thus, the passband generated by Mode 1 can be controlled by the parameter h accordingly. Therefore, the Mode 1 of SSPPs can be used to generate an adjustable passband with bandpass response.

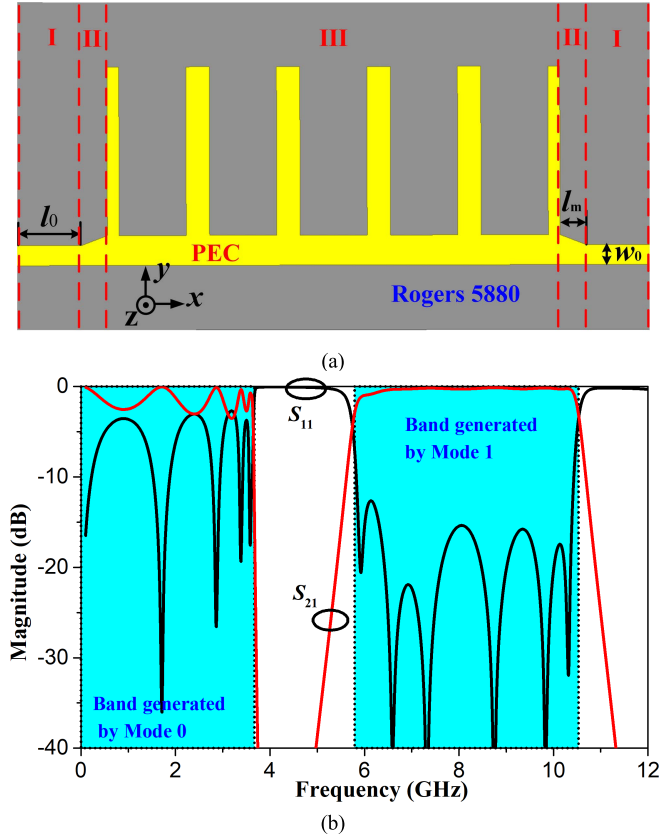


Fig. 4. (a) Schematic configuration and (b) simulated S -parameters of the proposed SSPP waveguide. The detailed dimensions are $l_0 = 5$ mm, $w_0 = 1.54$ mm, and $l_m = 2$ mm. The other parameters can refer to the SSPP unit cell in Fig. 1.

In order to generate the passband developed from Mode 1, a high-order SSPP waveguide at microwave frequency is constructed, as shown in Fig. 4(a), which is fed by microstrip lines to facilitate measurement. It is composed by three regions. The region I is a microstrip-line waveguide with 50- Ω characteristic impedance. The region II is a simple trapezoidal transition that seamlessly connects the microstrip line with the proposed SSPP structure, which only occupies very small space. As a mode-conversion transition, the length l_m of the trapezoidal structure is optimized to match the momentum of microstrip line to the SSPP waveguide smoothly. The region III is the SSPP structure consisting of five identical unit cells which have the same parameters as those of the unit cell in Fig. 1. The back of this waveguide is covered by the metallic ground plane.

Fig. 4(b) illustrates the simulated S -parameters of the proposed SSPP waveguide, where a bandpass filtering response is generated as expected with the lower and upper band edge of the passband at 5.79 and 10.53 GHz, respectively. These two frequencies are basically consistent with the frequency point of intersection 5.80 GHz and asymptotic frequency 10.65 GHz of Mode 1 in Fig. 1. Though the low-pass band from 0 to 3.6 GHz is yielded by Mode 0, the insertion loss is much worse than that of passband generated by Mode 1. The bandpass filtering response has good transmission performance with the minimal insertion loss of 0.16 dB, as well as the -12.6-dB reflection

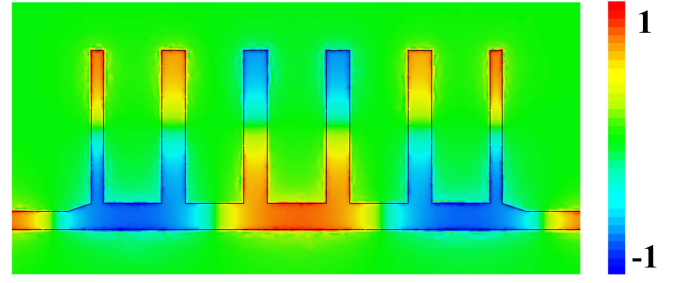


Fig. 5. Normalized electric field distribution on the xy plane of the high-order SSPP waveguide at 8 GHz.

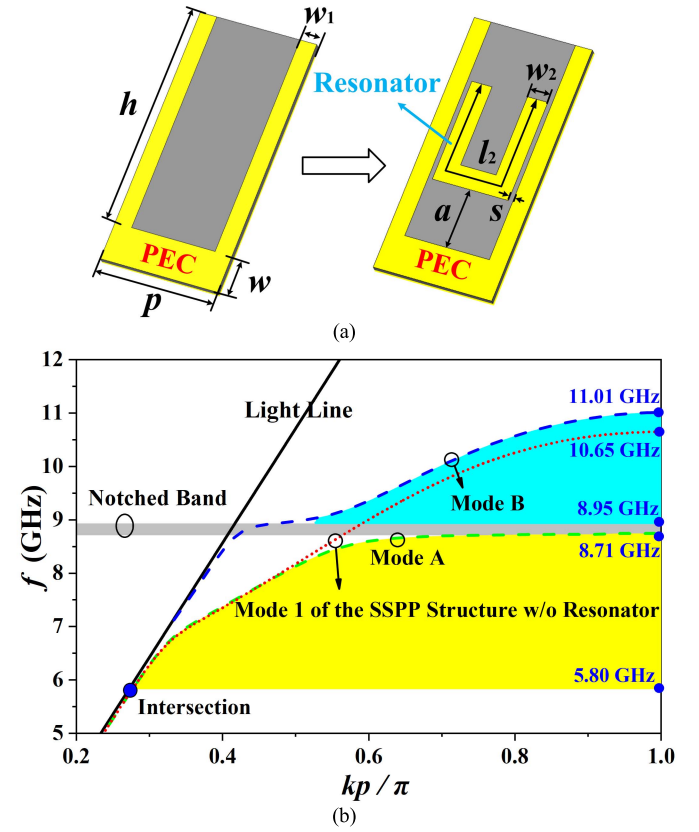


Fig. 6. (a) Schematic of the proposed SSPP unit cell and (b) its corresponding simulated dispersion characteristics when the parameters are set as $a = 3.5$ mm, $s = 0.25$ mm, $l_2 = 13$ mm, and $w_2 = 1.2$ mm. The other parameters are the same as those of the SSPP unit cell in Fig. 1.

coefficient. Note that the bandpass filtering performance is not worsened even if a very simple trapezoidal transition structure between the microstrip line and SSPP structure is employed for the mode conversion.

To further verify the propagation characteristics of the high-order mode of SSPPs, the electric field distribution of the SSPP waveguide at 8 GHz is depicted in Fig. 5. It can be seen that the energy is effectively transmitted from the input port to output port, and the electric field pattern is similar to the mode pattern in Fig. 2(b), i.e., the Mode 1 of SSPPs. Therefore, the high-efficiency passband can be obtained due to the successful excitation of the Mode 1.

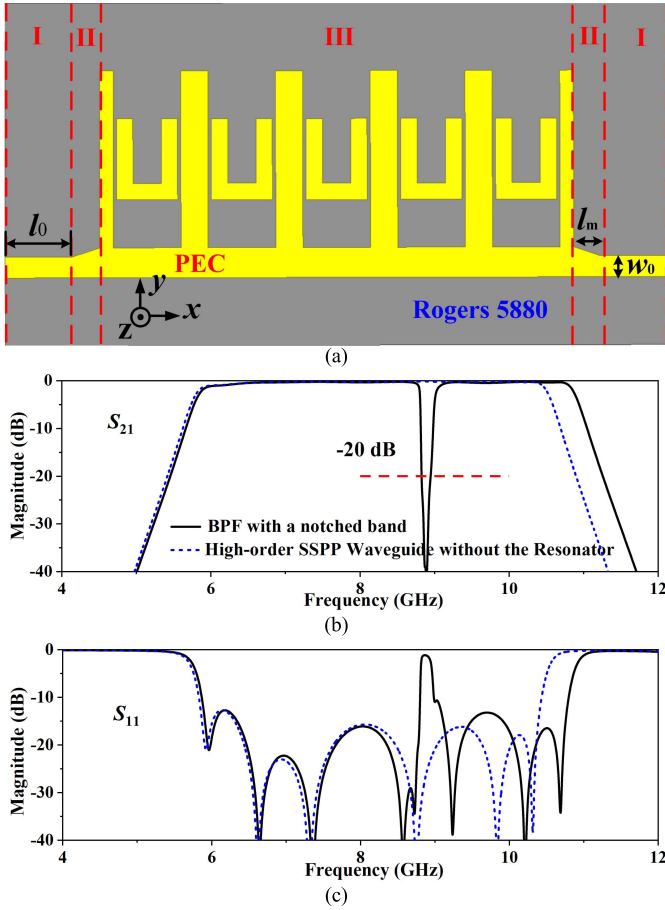


Fig. 7. (a) Schematic configuration, (b) simulated S_{21} and (c) simulated S_{11} of the designed BPF with a notched band.

B. BPF With a Notched Band

In this subsection, by embedding a U-shaped resonator into the SSPP unit cell, a new structural unit cell is constructed without occupying extra space, as shown in Fig. 6(a). It is analyzed by the dispersion characteristics in detail. Then, based on this proposed unit cell, a BPF with a notched band is designed with good performance as well as adjustable notch.

Based on the simulation of eigenmodes, the dispersion curve of this designed unit cell is acquired, as shown in Fig. 6(b). Moreover, the dispersion curves of the light line (black solid line) and the Mode 1 of high-order SSPP structure without the resonator (red dotted line) are introduced for reference. After adding the resonator, the Mode 1 is basically split to two parts, labeled as Mode A and Mode B, by a notched band where the SSPP mode cannot be supported. In order to give a clear observation, the regions covered by Mode A and Mode B are marked in yellow and blue, respectively, as well as the notched band region is marked in gray. As can be seen, the Mode A, covering from 5.80 to 8.71 GHz, has the same origin with the Mode 1. The asymptotic frequency of Mode B becomes slightly higher than that of Mode 1 due to interference of the added resonator. Consequently, the Mode B has the covering frequency from 8.95 to 11.01 GHz. Between the Mode A and Mode B, a notched band appears with the frequency range from 8.71 to 8.95 GHz, approximately corresponding to the resonant frequency of the half-wavelength U-shaped resonator.

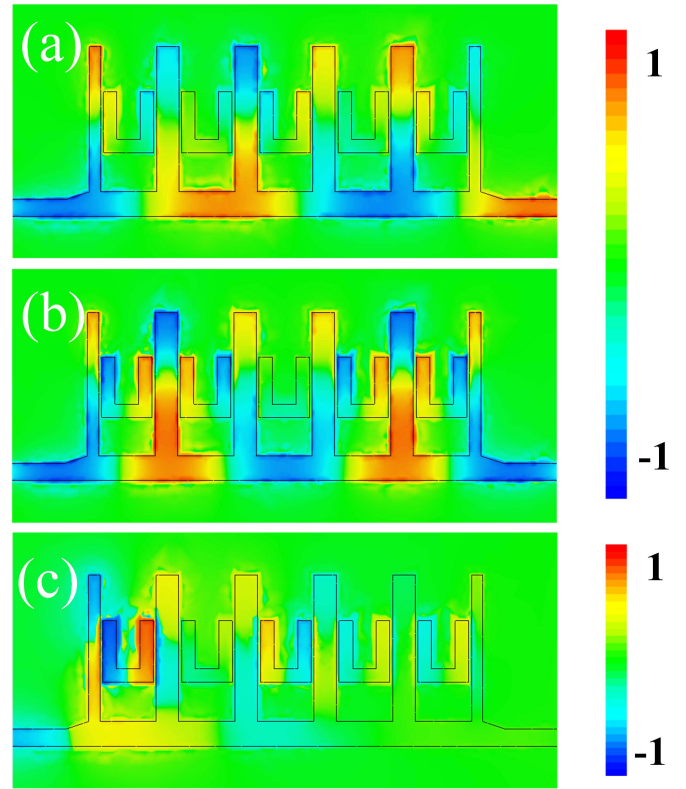


Fig. 8. Normalized electric field distributions of the proposed BPF at the frequencies of (a) 8 GHz, (b) 10 GHz, and (c) 8.9 GHz.

According to this feature, a BPF with a notched band will be designed below.

As presented in Fig. 7(a), the U-shaped resonator array is embedded into the SSPP waveguide to construct the proposed BPF with a notched band. The simulated transmission (S_{21}) and reflection (S_{11}) coefficients are investigated by frequency domain solver Ansys HFSS [32], and are plotted in Fig. 7(b) and (c), respectively. Also, the S -parameters of the corresponding high-order SSPP waveguide without resonator are plotted for reference. It is observed that a sharp notch is generated at the aimed frequencies as predicted in the dispersion curves. The notched band has the rejection level of -20 dB ranging from 8.81 to 8.94 GHz. In addition, the proposed BPF with a notched band has the same propagation performance as that of high-order SSPP waveguide without embedded resonator, except the notch band and upper band edge of the passband. For the passband's upper band edge, a slight blue shift happens, which is consistent with the dispersion characteristics in Fig. 6(b).

Furthermore, to give a clear insight into the transmission feature, the electric field distributions at 8, 10, and 8.9 GHz are depicted in Fig. 8. Due to the resonance of the embedding resonator at around 8.9 GHz, the electric field strength is primarily concentrated on the first resonator. The maximum of the electric field strength at 8.9 GHz is almost ten times of the ones at 8 and 10 GHz; therefore, the electric field at 8.9 GHz normalized into its maximum is different from the ones at 8 and 10 GHz. In the cases of 8 and 10 GHz located at the passband, the guided wave in microstrip line is effectively

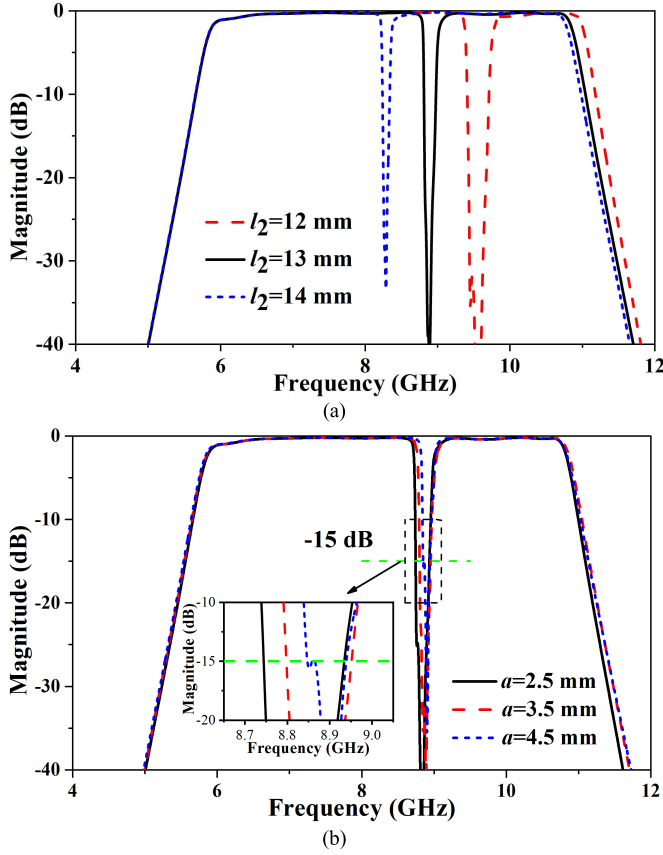


Fig. 9. Simulated S_{21} of the proposed BPF against (a) parameter l_2 and (b) parameter a .

transformed into SSPP mode; thus, the passband with good transmission performance is achieved. A difference should be noted that the embedded resonator is almost inactivated at 8 GHz in Fig. 8(a), while it is activated at 10 GHz in Fig. 8(b). This means that the resonator almost does not affect the signal propagation from input to output ports at lower frequencies. In contrast, the resonator will make the asymptotic frequency of the SSPP high-order mode higher than before, resulting in a blue shift for the upper band edge of the passband. At the frequency of 8.9 GHz, locating within the notched band, most of the electric field is concentrated on the first resonator; thus, the signals at the frequency of the notched band will be blocked.

Fig. 9(a) shows the transmission properties of the designed BPF with the varied l_2 , while other parameters are fixed. Here, l_2 denotes the overall length of U-shaped resonator, and we only tune the depth of U-shaped resonator but keep its width constant due to the fixed gap parameter s , as shown in Fig. 6(a). As l_2 increases from 12 to 14 mm, the notched band will be red-shifted. Meanwhile, the transmission performance of passband is rarely affected except the slight movement of the upper band edge. Consequently, the notched band of the proposed BPF can be conveniently adjusted by changing the value of l_2 to satisfy different application scenarios. Moreover, Fig. 9(b) presents the simulated S_{21} with the varied parameter a . It can be seen that the bandwidth of the notched band can be tuned to some extent by controlling the parameter a .

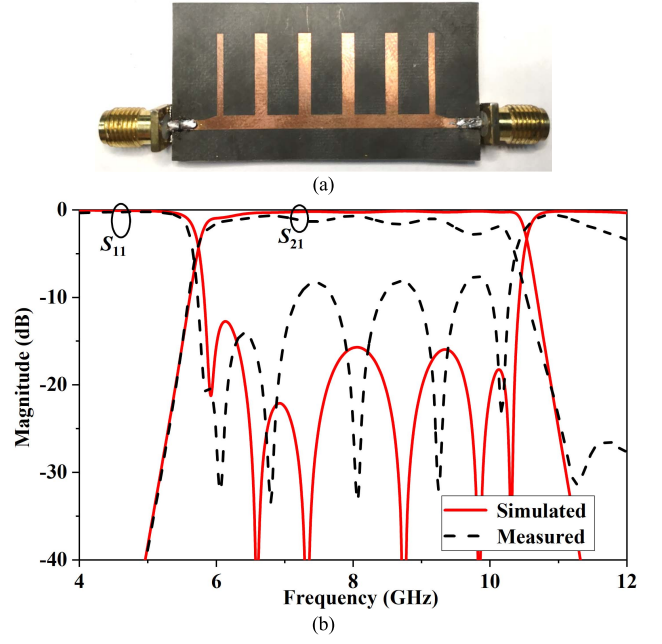


Fig. 10. (a) Fabricated SSPP waveguide using high-order mode and (b) its measured results compared with the simulated results.

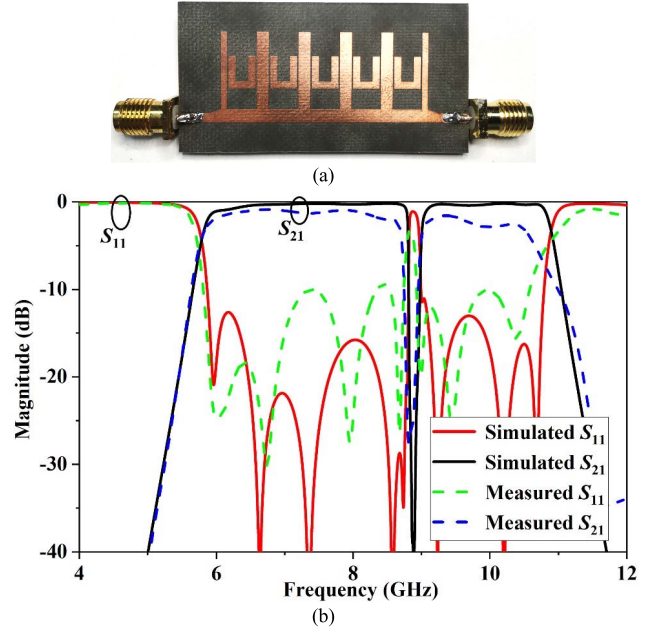


Fig. 11. (a) Fabricated BPF with a notched band and (b) its measured results compared with the simulated results.

III. EXPERIMENTAL RESULTS

In order to demonstrate the feasibility of our design, two abovementioned models have been fabricated and experimentally tested. Figs. 10(a) and 11(a) show the top view of the fabricated SSPP waveguide and BPF with a notched band, respectively. The two SMA connectors, connecting the 50- Ω microstrip lines, are welded to the both ends of two fabricated prototypes for measurement.

Their measured results are plotted in Figs. 10(b) and 11(b), respectively, in good agreement with the simulated results. It should be noted that the measured return loss and insertion loss at high frequency of the passband are a little higher than

the simulated ones. These discrepancies may be caused by the imperfect soldering and manufacturing tolerance at the high frequency.

IV. CONCLUSION

In this article, two SSPP-based BPFs without and with a notched band are presented using high-order SSPP modes. The high-efficiency passband originated from the Mode 1 of the SSPPs and the notched band generated by the embedding resonator are analyzed in detail. Two fabricated prototypes both have agreements between the simulated and measured results, which validate the feasibility of our design. Due to the simple structures and design method, the proposed work may have promising potential applications in plasmonic devices and systems.

REFERENCES

- [1] W. L. Barnes, A. Dereux, and T. W. Ebbesen, "Surface plasmon sub-wavelength optics," *Nature*, vol. 424, no. 6950, pp. 824–830, Aug. 2003.
- [2] M. Marklund, G. Brodin, L. Stenflo, and C. S. Liu, "New quantum limits in plasmonic devices," *EPL Europhys. Lett.*, vol. 84, no. 1, p. 17006, Oct. 2008.
- [3] K. Arshad, M. Lazar, S. Mahmood, Aman-ur-Rehman, and S. Poedts, "Kinetic study of electrostatic twisted waves instability in nonthermal dusty plasmas," *Phys. Plasmas*, vol. 24, no. 3, Mar. 2017, Art. no. 033701.
- [4] K. Arshad, "Application of kinetic theory to study twisted modes in non-Maxwellian plasmas," Ph.D. dissertation, Dept. Sci., KU Leuven, Leuven, Belgium, 2018.
- [5] D. K. Gramotnev and S. I. Bozhevolnyi, "Plasmonics beyond the diffraction limit," *Nature Photon.*, vol. 4, no. 2, pp. 83–91, Jan. 2010.
- [6] E. Ozbay, "Plasmonics: Merging photonics and electronics at nanoscale dimensions," *Science*, vol. 311, no. 5758, pp. 189–193, Jan. 2006.
- [7] J. B. Pendry, "Mimicking surface plasmons with structured surfaces," *Science*, vol. 305, no. 5685, pp. 847–848, Aug. 2004.
- [8] F. J. Garcia-Vidal, L. Martín-Moreno, and J. B. Pendry, "Surfaces with holes in them: New plasmonic metamaterials," *J. Opt. A, Pure Appl. Opt.*, vol. 7, no. 2, pp. S97–S101, Feb. 2005.
- [9] A. P. Hibbins, "Experimental verification of designer surface plasmons," *Science*, vol. 308, no. 5722, pp. 670–672, Apr. 2005.
- [10] Y.-Q. Liu, L.-B. Kong, C.-H. Du, and P.-K. Liu, "A terahertz electronic source based on the spoof surface plasmon with subwavelength metallic grating," *IEEE Trans. Plasma Sci.*, vol. 44, no. 6, pp. 930–937, Jun. 2016.
- [11] Y.-Q. Liu, C.-H. Du, and P.-K. Liu, "Terahertz electronic source based on spoof surface plasmons on the doubly corrugated metallic waveguide," *IEEE Trans. Plasma Sci.*, vol. 44, no. 12, pp. 3288–3294, Dec. 2016.
- [12] J.-F. Zhu, C.-H. Du, L.-Y. Bao, and P.-K. Liu, "Regenerated amplification of terahertz spoof surface plasmon radiation," *New J. Phys.*, vol. 21, no. 3, Mar. 2019, Art. no. 033021.
- [13] X. Shen, T. J. Cui, D. Martín-Cano, and F. J. Garcia-Vidal, "Conformal surface plasmons propagating on ultrathin and flexible films," *Proc. Nat. Acad. Sci. USA*, vol. 110, no. 1, pp. 40–45, Jan. 2013.
- [14] X. Shen and T. Jun Cui, "Planar plasmonic metamaterial on a thin film with nearly zero thickness," *Appl. Phys. Lett.*, vol. 102, no. 21, May 2013, Art. no. 211909.
- [15] H. F. Ma, X. P. Shen, Q. Cheng, W. X. Jiang, and T. J. Cui, "Broadband and high-efficiency conversion from guided waves to spoof surface plasmon polaritons," *Laser Photon. Rev.*, vol. 8, no. 1, pp. 146–151, 2014.
- [16] Y.-J. Guo, K.-D. Xu, and X. Deng, "Tunable enhanced sensing of ferrite film using meander-shaped spoof surface plasmon polariton waveguide," *Appl. Phys. Exp.*, vol. 12, no. 11, Nov. 2019, Art. no. 115502.
- [17] Y.-J. Guo, K.-D. Xu, X. Deng, X. Cheng, and Q. Chen, "Millimeter-wave on-chip bandpass filter based on spoof surface plasmon polaritons," *IEEE Electron Device Lett.*, vol. 41, no. 8, pp. 1165–1168, Aug. 2020.
- [18] K.-D. Xu, F. Zhang, Y.-J. Guo, L. Ye, and Y. Liu, "Spoof surface plasmon polaritons based on balanced coplanar stripline waveguides," *IEEE Photon. Technol. Lett.*, vol. 32, no. 1, pp. 55–58, Dec. 2020.
- [19] W. Feng, Y. Feng, W. Yang, W. Che, and Q. Xue, "High-performance filtering antenna using spoof surface plasmon polaritons," *IEEE Trans. Plasma Sci.*, vol. 47, no. 6, pp. 2832–2837, Jun. 2019.
- [20] J. Wang, L. Zhao, Z. C. Hao, X. P. Shen, and T. J. Cui, "Splitting spoof surface plasmon polaritons to different directions with high efficiency in ultra-wideband frequencies," *Opt. Lett.*, vol. 44, no. 13, pp. 3374–3377, Jul. 2019.
- [21] C. Han, Z. H. Wang, Y. Y. Chu, X. D. Zhao, and X. R. Zhang, "Compact flexible multifrequency splitter based on plasmonic graded metallic grating arc waveguide," *Opt. Lett.*, vol. 43, no. 8, pp. 1898–1901, 2018.
- [22] D. Zhang, K. Zhang, Q. Wu, R. Dai, and X. Sha, "Broadband high-order mode of spoof surface plasmon polaritons supported by compact complementary structure with high efficiency," *Opt. Lett.*, vol. 43, no. 13, pp. 3176–3179, Jul. 2018.
- [23] K. D. Xu, Y. J. Guo, and X. Deng, "Terahertz broadband spoof surface plasmon polaritons using high-order mode developed from ultra-compact split-ring grooves," *Opt. Exp.*, vol. 27, no. 4, pp. 4354–4363, Feb. 2019.
- [24] T. Jiang, L. Shen, X. Zhang, and L.-X. Ran, "High-order modes of spoof surface plasmon polaritons on periodically corrugated metal surfaces," *Prog. Electromagn. Res. M*, vol. 8, pp. 91–102, 2009.
- [25] X. Liu, Y. Feng, B. Zhu, J. Zhao, and T. Jiang, "High-order modes of spoof surface plasmonic wave transmission on thin metal film structure," *Opt. Exp.*, vol. 21, no. 25, pp. 31155–31165, 2013.
- [26] Q. Zhang, H. C. Zhang, J. Y. Yin, B. C. Pan, and T. J. Cui, "A series of compact rejection filters based on the interaction between spoof SPPs and CSRRs," *Sci. Rep.*, vol. 6, no. 1, Sep. 2016, Art. no. 28256.
- [27] Y. J. Zhou and Q. X. Xiao, "Electronically controlled rejections of spoof surface plasmons polaritons," *J. Appl. Phys.*, vol. 121, no. 12, Mar. 2017, Art. no. 123109.
- [28] L. Ye *et al.*, "Super subwavelength guiding and rejecting of terahertz spoof SPPs enabled by planar plasmonic waveguides and notch filters based on spiral-shaped units," *J. Lightw. Technol.*, vol. 36, no. 20, pp. 4988–4994, Oct. 15, 2018.
- [29] L. P. Li, P. Chen, P. F. Zhu, and K. Yang, "A compact rejection filter based on spoof surface plasmon polaritons and folded split-ring resonators with controllable rejection bandwidth," *Appl. Comput. Electromagn. Soc. J.*, vol. 34, no. 9, pp. 1405–1410, 2019.
- [30] Rogers Corporation. *Advanced Connectivity Solutions*. [Online]. Available: <https://www.rogerscorp.com/-/media/project/rogerscorp/documents/advanced-connectivity-solutions/english/data-sheets/rt-duroid-5870-5880-data-sheet.pdf>
- [31] Y. J. Guo, K. D. Xu, and X. Tang, "Spoof plasmonic waveguide developed from coplanar stripline for strongly confined terahertz propagation and its application in microwave filters," *Opt. Exp.*, vol. 26, no. 8, pp. 10589–10598, Apr. 2018.
- [32] *Ansys High Frequency Structure Simulator (HFSS)*. [Online]. Available: <https://www.ansys.com/products/electronics/ansys-hfss>



Kai-Da Xu (Senior Member, IEEE) received the B.E. and Ph.D. degrees in electromagnetic field and microwave technology from the University of Electronic Science and Technology of China (UESTC), Chengdu, China, in 2009 and 2015, respectively.

From 2012 to 2014, he was a Visiting Researcher with the Department of Electrical and Computer Engineering, Duke University, Durham, NC, USA, under the financial support from the China Scholarship Council. In 2015, he joined the Department of Electronic Science, Xiamen University, Xiamen, China, as an Assistant Professor. From 2016 to 2017, he was a Post-Doctoral Fellow with the State Key Laboratory of Millimeter Waves, City University of Hong Kong, Hong Kong. From 2018 to 2019, he was an Honorary Fellow with the Department of Electrical and Computer Engineering, University of Wisconsin–Madison, WI, USA. In 2020, he joined the School of Information and Communications Engineering, Xi'an Jiaotong University (XJTU). He has authored and coauthored over 100 papers in peer-reviewed journals and over 40 papers in conference proceedings. His current research interests include RF/microwave, mm-wave/THz devices, and antenna arrays.

Dr. Xu was awarded a fellowship from the Japan Society for the Promotion of Science (JSPS) and joined the Department of Communications Engineering, Graduate School of Engineering, Tohoku University, as the JSPS Fellow in November 2019. He received the UESTC Outstanding Graduate Awards in 2009 and 2015, respectively. He was a recipient of the National Graduate Student Scholarship in 2012, 2013, and 2014 from the Ministry of Education, China. He was successfully selected into the "Youth Talent Support Program" of XJTU in 2019. Since 2017, he has been served as an Associate Editor for both of the *IEEE Access* and *Electronics Letters*. He is also an Editorial Board Member of the *AEÜ-International Journal of Electronics and Communications*.



Sen Lu was born in Shandong, China, in 1996. He received the B.Eng. degree in electronic information and engineering from Northeastern University, Qinhuangdao, China, in 2018. He is currently pursuing the M.Eng. degree with the Department of Electronic Science, Xiamen University, Xiamen, China.

His current research interests include RF and microwave passive components.



Ying-Jiang Guo received the B.E. degree in electronic engineering from Sichuan University, Chengdu, China, in 2008, and the Ph.D. degree from the University of Electronic Science and Technology in China, Chengdu, China, in 2018.

From 2011 to 2013, he was with Huawei Technologies Company, Ltd., Shenzhen, China, where he was involved in the research on 5G communication prototype design. From 2013 to 2014, he was with Sichuan Normal University, Chengdu, China, where he was a Lecturer. Since 2018, he has been

with Microsystem and Terahertz Research Center in China Academy of Engineering Physics as an Assistant Research Fellow and focuses on the terahertz integrated circuits and communication technologies. He has authored or coauthored over 30 journal and conference papers. He holds over five patents in wireless communication. His current research interests include the RF/microwave/mm-wave integrated circuits, THz modules/antennas, and systems in package.



Qiang Chen (Senior Member, IEEE) received the B.E. degree from Xidian University, Xi'an, China, in 1986, and the M.E. and D.E. degrees from Tohoku University, Sendai, Japan, in 1991 and 1994, respectively.

He is currently the Chair Professor of Electromagnetic Engineering Laboratory with the Department of Communications Engineering, School of Engineering, Tohoku University. His primary research interests include antennas, microwave and millimeter wave, antenna measurement, and computational

electromagnetics.

Dr. Chen is the IEICE Fellow. He received the Best Paper Award and Zen-ichi Kiyasu Award in 2009 from the Institute of Electronics, Information and Communication Engineers (IEICE). He served as the Chair of IEICE Technical Committee on Photonics-Applied Electromagnetic Measurement from 2012 to 2014, the Chair of IEICE Technical Committee on Wireless Power Transfer from 2016 to 2018, and the Chair of Tokyo Chapter of IEEE Antennas and Propagation Society from 2017 to 2018. He is currently the Chair of IEICE Technical Committee on Antennas and Propagation.